

# DCNAS: Densely Connected Neural Architecture Search for Semantic Image Segmentation

Xiong Zhang<sup>1</sup>, Hongmin Xu<sup>2</sup>, Hong Mo<sup>3</sup>, Jianchao Tan<sup>2</sup>, Cheng Yang<sup>1</sup>, Wenqi Ren<sup>4</sup>

<sup>1</sup>JOYY Inc., <sup>2</sup>Y-tech, Kwai, <sup>3</sup>Beihang University, <sup>4</sup>SKLOIS, IIE, CAS

**Abstract.** Neural Architecture Search (NAS) has shown great potentials in automatically designing scalable network architectures for dense image predictions. However, existing NAS algorithms usually compromise on restricted search space and search on proxy task to meet the achievable computational demands. To allow as wide as possible network architectures and avoid the gap between target and proxy dataset, we propose a Densely Connected NAS (**DCNAS**) framework, which directly searches the optimal network structures for the multi-scale representations of visual information, over a large-scale target dataset. Specifically, by connecting cells with each other using learnable weights, we introduce a densely connected search space to cover an abundance of mainstream network designs. Moreover, by combining both path-level and channel-level sampling strategies, we design a fusion module to reduce the memory consumption of ample search space. We demonstrate that the architecture obtained from our DCNAS algorithm achieves state-of-the-art performances on public semantic image segmentation benchmarks, including 83.6% on Cityscapes, and 86.9% on PASCAL VOC 2012 (track w/o additional data). We also retain leading performances when evaluating the architecture on the more challenging ADE20K and Pascal Context dataset.

**Keywords:** neural architecture search, NAS, semantic image segmentation, scene parsing, multi-scale feature fusion

## 1 Introduction

The heavy computation overheads of early Neural Architecture Search (NAS) methods [1] hinder their applications to real-world problems. Recently, limited search space strategies [2,3,4] significantly shorten the searching time of NAS algorithms, which make NAS approaches achieve superhuman performance in image classification tasks. However, to meet the low consumption of searching time, those constrained search space NAS methods throw down the multi-scale representations of high-resolution image. As a result, those methods are not suitable for dense image prediction tasks (*e.g.* semantic image segmentation, object detection and monocular depth estimation).

To efficiently search appropriate network structures that can combine both the local and global clues of the input image, researches recently focus on improving NAS frameworks by designing new search spaces to handle multi-scale features. For instance, DPC [5] introduces a recursive search space, and Auto-DeepLab [6] proposes a hierarchical search space and so on. However, designing new search space for dense image prediction tasks is challenging: one has to delicately compose a flexible search space that covers as much as possible optimal network architectures. Meanwhile, efficiently address memory consumption and the heavy computation problems accompanied with ample search space for the high-resolution imagery.

In this work, we propose an efficient and proxyless NAS framework to search the optimal model structure for semantic image segmentation. Our approach is based on two principal considerations. Firstly, the search space should be comprehensive enough to handle most of the mainstream architecture’s designs, even some undiscovered high-quality model structures. Unlike previous works [6,7,8,9,10] that explore promising model structures in reduced search spaces, as shown in Figure 1, we design a reticular-like and fully densely connected search space, which contains various paths in the search space. Consequently, DCNAS may derive whichever model architecture designs (*e.g.*, U-net [11], HourGlass [12]) by selecting appropriate paths among the whole set of these connections. Additionally, DCNAS aggregate contextual semantics encoded in multi-scale imageries to derive long-range context information, which has been recently found to be vital to the state-of-the-art manually designed image segmentation models [13,14,15,16,17]. Secondly, we observe that previous NAS approaches [5,6] heavily rely on the proxy task or proxy dataset to reduce the cost of GPU hours and to alleviate the high GPU memory consumption problem. However, architectures optimized over proxy are not guaranteed to be also suitable in realistic setting [18], because of the gap between the proxy and the target configuration. Regarding this concern, we draw on the experience of continuous relaxation that relaxes the discrete architectures into continuous representation to save GPU hours and design a fusion module which applies both path-level and channel-level sampling strategies during the searching procedure, to reduce memory demand. Based on that, we can employ the stochastic gradient descent (SGD) to perform the proxyless searching procedure to select the optimal architecture from all the candidate models without the help of proxy datasets or proxy tasks. The searching procedure takes about 5.6 GPU days on Cityscapes [19] dataset.

We apply our proposed approach to semantic image segmentation tasks on several public benchmarks, our model achieves the best performance compared with state-of-the-art hand-craft models [20,14,21,16,22,23,24] and other contemporary NAS approaches [6,5]. We also evaluate the optimal model identified by DCNAS on Pascal VOC 2012 [25], the model outperforms other leading approaches [26,24,14,27,28,29,17,30] and advances the state-of-the-art performance without using additional data. Transferring the model to ADE20K [31] and PASCAL-Context [32] datasets, our model obtains the best result compared

with state-of-the-art approaches [23,24,33,22,34,28,35], according to the corresponding evaluation metrics.

To summarize, our main contributions are as follows:

- We design a first entirely densely connected search space, which allows to explore various existing designs and is capable of covering arbitrary model architecture patterns.
- We implement the first proxyless searching paradigm to efficiently and directly explore the most promising model among all the candidates encoded in DCNAS, on large-scale segmentation datasets (*e.g.*, Cityscapes [19]).
- We demonstrate new state-of-the-art performance on Cityscapes [19], PASCAL-VOC 2012 [25], Pascal-Context [32] and ADE20K [31] datasets.

## 2 Related Work

### 2.1 Neural Architecture Search Space

Early NAS works [1,36] directly search the whole network architecture. Although those works achieve impressive results, their expensive computation overheads (*e.g.* thousands of GPU days) hinder their applications in real-world scenarios. To alleviate this situation, researchers proposed restricted search space methods. NASNet [2] first proposed a cell-based search space. Concretely, NASet searches the best cell structure, which is easier than searches the whole network architectures on a small proxy dataset. Then it repeats to stack the searched best cell to construct a new network on a large target dataset. After that, many works [4,37,18,38,39] adopt the cell-based search space design and make improvements in several ways. One line of works [18,38,39] attempt to search high-efficiency network architectures for resource-constrained platforms, such as mobile phones. Another line of works [40,41] try to improve previous cell-based NAS methods. P-DRATS [40] first bridge the depth gap between search and evaluation phases. Fang *et al.*[41] proposes the routing blocks to determine the number of blocks automatically.

Despite the success of repeated cell-based methods for image classification tasks, other dense image prediction tasks, such as semantic image segmentation and object detection, demand more delicate and complicated network architectures to capture multi-scale information of the image. Therefore, researchers begin to explore more flexible search space for dense image prediction tasks. For instance, DPC [5] proposes a recursive search space to build a multi-scale representation of a high-resolution image. Auto-DeepLab [6] introduces a hierarchical search space to exhibit multi-level representations of the image.

### 2.2 Semantic Image Segmentation

The pioneer work FCNs [11] makes great progress in semantic segmentation by introducing a fully convolutional network. Afterwards, researchers devote enormous efforts to explore the tremendous potentials of convolutional neural

networks (CNNs) on dense image prediction tasks. Several kinds of research works [14,42,43,44,45,46,12,47,48,16,49] focus on how to efficiently utilize multi-scale context information to improve the performance of semantic segmentation systems. Some works [42,43,44] takes an image pyramid as input to capture larger objects in down-sampled input image. Some other works try to make use of multi-scale context information. PSPNet [14] uses spatial pyramid pooling at different manually set scales. Deeplab [45] performs multiple rates atrous convolution operations. Also, there are some works [46,12,47,48,16,49] that employ encoder-decoder structure to captures long-range context information.

Most above mentioned research works focus on handcrafting network structures to take good advantages of context information. Most recently, some works [5,6,8,9,7,50,10,51] shift from manually design network architecture to automatically ones. Research works, such as [8,9,7,50,10,51], target to search network structures that are friendly to resource-constrained devices for semantic segmentation task. Some other works, such as DPC [5] and Auto-DeepLab [6], intent to directly search the highest-performance network architecture for semantic segmentation without considering computation overheads. Most of those works [6,8,9,7,50,10,51] suffer from limited search space and search on proxy tasks, because of high GPU memory consumption and expensive computational burden. Yet the optimal network structures for multi-scale feature representations require ample search space.

The most similar works to ours are DPC [5] and Auto-DeepLab [6]. DPC proposes an ample search space but requires thousands of GPU days searching time, whereas we can efficiently search over at least the same search space using only 5.6 GPU days. Auto-DeepLab has comparable searching time like ours, yet contains a smaller search space than ours. Besides, both DPC and Auto-DeepLab search on the proxy dataset, whereas we can directly search on the target dataset.

### 3 Methods

The main goal of this work is to propose an efficient and proxyless framework to automatically design models for semantic image segmentation tasks. In this section, we introduce several vital components of the framework in details, including a densely connected search space that is general enough to cover whichever network design paradigms, the derived continuously differentiable representation of the novel search space, and the approach that can save the cost of GPU hours and reduce the excessive memory footprint.

#### 3.1 Densely Connected Search Space

The densely connected search space (DCSS) involves two primitives, the *mixture layer*, and the *fusion module*. The *mixture layer* is defined as a mixture of the candidate operators, and the *fusion module* aims at aggregating semantic features from preceding fusion modules. A range of reticular-like and densely

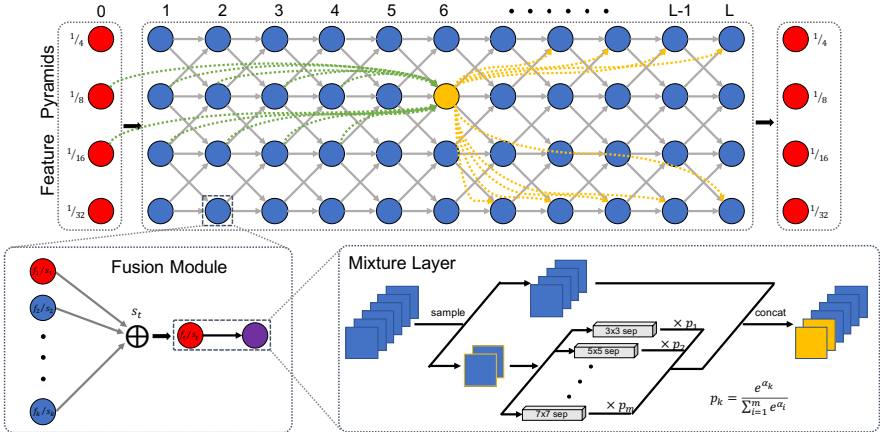


**Fig. 1. Densely Connected Search Space (DCSS).** The DCSS is a reticular-like search space that aims to fuse the multi-scale semantic features, the dense connections make it general enough to handle whatever architecture patterns. One may obtain any model structure by selecting the appropriate connections embedded in DCSS and assigning proper operations for each layer. Note that, for simplicity, we take the golden node as an example and demonstrate several associated dense connections.

connected fusion modules constitute the architecture of DCSS, as shown in Figure 1.

**Mixture Layer.** The *mixture layer* is the elementary structure in our search space that represents a collection of available operations. In this work, we exploit the MobileNetV3 [52] entity to build the operator spaces. Similar to [18], we construct the operator space  $\mathcal{O}$  with various configurations of MobileNetV2 plus Squeeze-and-Excite structure, *i.e.*, kernel sizes  $k \in \{3, 5, 7\}$ , expansion ratios  $r \in \{3, 6\}$ . Due to the dense connections contained in the search space, the DCSS inherently supports the zero operation and identity operation. Hence  $\mathcal{O}$  does not contain the above operations explicitly. Considering that the DCSS inherently favors the multi-scale semantic features aggregation, which increase the receptive field, therefore, the mixture layer does not support atrous convolution explicitly.

**Fusion Module.** To explore various paths in DCSS, we introduce the *fusion module* with the ability of aggregating semantic features from preceding fusion modules besides the feature pyramids and attaching transformed semantic features to succeeding ones. As illustrated by the bottom-left part in Figure 1, the fusion model consists of the shape-alignment layer besides the mixture layer. The shape-alignment layer is in a multi-branch parallel form. Given an array of feature-maps with different shapes (*e.g.*, spatial resolutions and channel widths), the shape-alignment layer dispatches each feature-map to the corresponding branches to align them to the target shape. Semantic features are well-aligned and fully aggregated, then feed into the mixture layer to perform efficient multi-scale features fusion.

**Search Space.** Benefiting from the sophisticated design of the fusion module, we introduce a set of reticular-arranged fusion modules and place dense connections between them to form a general search space that supports more flexible architecture configurations than similar work of [6]. The search algorithm is admitted to select a subset of the fusion models together with the appropriate connections between them to derive whatever model architecture, hence enables a general architecture search. Specifically, we construct the super network with an array of fusion modules  $\{\mathcal{M}_{(s,l)}\}$ , where  $s \in \mathbb{S}$  indicate the spatial configuration and  $l \in \mathbb{L}$  refers to the layer index, which is demonstrated in Figure 1. For those fusion modules in the same row, the width of the input feature-maps stays the same, while the spatial resolution of the inputs keeps the same for fusion modules within the same column. Each fusion module  $\mathcal{M}_{(s,l)}$  aggregates the semantic features coming from  $\{\mathcal{M}_{(s',l')} \mid l' < l\}$  in addition to the feature pyramids.

### 3.2 Differentiable Representation

Reinforcement learning representations in [53,1] and evolutionary representations in [54,36] both tend to be computationally intensive, hence probably not suitable for semantic image segmentation tasks. Regarding this concern, we draw on the experience of continuous relaxation in [4,55] and relax the discrete architectures into continuous representation. Notably, we derive a continuous representation for both the mixture layer and the fusion module, hence leading to a fully differentiable search space, based on which one can apply the stochastic gradient descent method to search promising architectures.

**Mixture Layer.** We assign an architecture parameter  $\alpha_{(s,l)}^o$  to the candidate operator  $o$  in mixture layer  $\ell_{(s,l)}$  contained in fusion module  $\mathcal{M}_{(s,l)}$ , one may derive the continuously representation of the mixture layer by defining it as a weighted sum of outputs from all candidate operations. The architecture weight of the operation is computed as a soft-max of architecture parameters over all operations in the mixture layer:

$$w_{(s,l)}^o = \frac{\exp\left(\alpha_{(s,l)}^o\right)}{\sum_{o' \in \mathcal{O}} \exp\left(\alpha_{(s,l)}^{o'}\right)}. \quad (1)$$

and the output of mixture layer  $\ell_{(s,l)}$  can be estimated as,

$$O_{(s,l)} = \sum_{o \in \mathcal{O}} w_{(s,l)}^o \cdot o\left(\mathcal{I}_{(s,l)}\right). \quad (2)$$

where  $\mathcal{I}_{(s,l)}$  refers to the input feature-maps of mixture layer  $\ell_{(s,l)}$ .

**Fusion Module.** Similar to the relaxation paradigm adopted in the mixture layer, to relax the connections as a continuous representation, we assign an architecture parameter  $\beta_{(s',l') \rightarrow (s,l)}$  for the path from  $\mathcal{M}_{(s',l')}$  to  $\mathcal{M}_{(s,l)}$ . Since the fusion module  $\mathcal{M}_{(s,l)}$  aggregates all semantic features  $\{\mathcal{I}_{(s',l')} \mid l' < l\}$ , we estimate

the transmission probability of each path using a soft-max function over all available connections:

$$p_{(s',l') \rightarrow (s,l)} = \frac{\exp \{ \beta_{(s',l') \rightarrow (s,l)} \}}{\sum_{s'' \in \mathbb{S}} \sum_{0 \leq l'' < n} \exp \{ \beta_{(s'',l'') \rightarrow (s,l)} \}}. \quad (3)$$

and the aggregating process can be formalized as:

$$\mathcal{I}_{(s,l)} = \sum_{s' \in \mathbb{S}} \sum_{l' < l} p_{(s',l') \rightarrow (s,l)} \cdot H_{(s',l') \rightarrow (s,l)}(O_{(s',l')}), \quad (4)$$

where  $H_{(s',l') \rightarrow (s,l)}$  denotes the corresponding transformation branch in shape-alignment layer of fusion module  $\mathcal{M}_{(s,l)}$ , which transforms the semantic features produced by mixture layer  $\ell_{(s',l')}$  to the shape specified by  $\mathcal{M}_{(s,l)}$ .

### 3.3 Reducing Memory Footprint

Continuous representation of network architectures can largely reduce the cost of GPU hours, while the memory footprint grows linearly w.r.t. the size of candidate operation set and the number of connections, hence suffering from the high GPU memory consumption problem. Image segmentation intrinsically requires high-resolution semantic features, which will lead to even more GPU memory consumption. To resolve the excessive memory consumption problem, some researchers make use of proxy tasks [4,55], *e.g.*, searching over a smaller search space, while other works make use of proxy dataset [6], *e.g.*, smaller or low-resolution images, to reduce the searching cost. However, the architectures optimized with proxy are not warranted to be optimal on the target task [18]. Taking these factors into account, we apply the sampling strategy both in the fusion module and the mixture layer to solve the excessive memory footprint problem and further reduce the cost of GPU hours. By taking the above tactics, one can proxylessly search the model over large-scale dataset instead of using a proxy, hence avoiding the gap between target and proxy dataset.

**Fusion Module.** The DCSS contains  $8L * (L + 1)$  connections in total, where  $L$  is layer number, thus making it impossible to optimize the whole set of candidate connections in each iteration because of the extravagant GPU memory demand. Therefore, in each iteration during the search, for each fusion module, we sample several connections among the corresponding potential connections. Concretely, taking fusion module  $\mathcal{M}_{(s,l)}$  for instance, all the preceding fusion modules  $\{ \mathcal{M}_{(s',l')} | 0 \leq l' < l \}$  are associated with it, in each search iteration, we perform sampling without replacement to activate several transmission paths, and the probability distribution is defined as:

$$p_{(s',l') \rightarrow (s,l)} = \frac{\exp \{ \beta_{(s',l') \rightarrow (s,l)} / \tau \}}{\sum_{0 \leq l'' < l} \sum_{s'' \in \mathbb{S}} \exp \{ \beta_{(s'',l'') \rightarrow (s,l)} / \tau \}}, \quad (5)$$

where  $\beta_{(s'',l'') \rightarrow (s,l)}$  share the same definition in Equation 3, and the temperature variable  $\tau$  starts from a high temperature then anneal to a small but non-zero

value. Assume there are  $n$  fusion modules  $\{\mathcal{M}_{(s_1, l_1)}, \mathcal{M}_{(s_2, l_2)}, \dots, \mathcal{M}_{(s_n, l_n)}\}$  selected from  $\{\mathcal{M}_{(s', l')} | 0 \leq l' < l\}$ , then we may approximate Equation 4 with:

$$\mathcal{I}_{(s, l)} = \sum_{1 \leq k < n} w_{(s_k, l_k) \rightarrow (s, l)} * H_{(s_k, l_k) \rightarrow (s, l)}(O_{(s_k, l_k)}), \quad (6)$$

where  $w_{(s_k, l_k) \rightarrow (s, l)}$  refers to the normalized blending weight,  $H$  and  $O$  shares the same definition in Equation 4.

**Mixture Layer.** A typical way to apply the sampling trick is to sample the operator  $o$  from the candidate operator space  $\mathcal{O}$  in each mixture layer. While in practice, we find that the naive sampling strategy makes the searching process unstable and sometime does not convergence. In stead, we introduce a novel strategy, which samples a portion of channels from the input features, then sends the lucky ones into the mixed transformation of  $|\mathcal{O}|$  operators while bypasses the others. Specifically, for each fusion layer  $\ell_{(s, l)}$ , we assign a dedicated random variable  $S_{(s, l)}$  that control the ratio of sampled channels, which trades off the search accuracy and efficiency, and we may rewrite the Equation 2 as:

$$O_{(s, l)} = \sum_{o \in \mathcal{O}} w_{(s, l)}^o \cdot o(S_{(s, l)} * \mathcal{I}_{(s, l)}) + (1 - S_{(s, l)}) * \mathcal{I}_{(s, l)}, \quad (7)$$

where  $w_{(s, l)}^o$  indicates the normalized blending weight defined by Equation 1. In particular, we do not tune the sampling ratio and fix it to be  $1/4$ , empirically, our experiments demonstrate that it works well. With this scheme, one can gain  $4 \times$  acceleration of the searching process, and save 75% GPU memory consumption.

### 3.4 Search Procedure

Benefiting from the fully differentiable representation of the search space and the sampling strategies mentioned above, one may apply the stochastic gradient descent algorithm to search for appropriate models by optimizing architecture parameters  $\{\alpha, \beta\}$  on the target dataset without proxy. Similar to previous works [4, 5, 6], we partition the training data into two parts *trainA* and *trainB*, which are used for updating the convolutional weights  $w$  and architecture parameters  $\{\alpha, \beta\}$  respectively. We solve this optimization problem alternatively:

- update convolutional weights  $w$  by  $\nabla_w \mathcal{L}_{trainA}(w, \alpha, \beta)$
- update architecture parameters  $\{\alpha, \beta\}$  by  $\nabla_{\alpha, \beta} \mathcal{L}_{trainB}(w, \alpha, \beta)$ .

in which the loss function  $\mathcal{L}$  mainly consists of the classical cross entropy calculated on each mini-batch.

We shall point out that, in practice,  $\mathcal{L}$  comprises of several practical regularization terms in addition to cross-entropy, experiments reveal that the regularization terms yield a faster convergence rate of the searching procedure and lead to a better searching accuracy. Practically, the beneficial regularization terms are listed below:



- 1 Since we may select the optimal operator  $\arg \max_{o \in \mathcal{O}} \alpha_{(s,l)}^o$ , we introduce the entropy regularization term  $\mathcal{L}_\alpha = - \sum_{o \in \mathcal{O}} \sum_{s \in \mathbb{S}} \sum_{l \in \mathbb{L}} w_{(s,l)}^o \ln w_{(s,l)}^o$  over architecture parameters  $\alpha$ .
- 2 The insignificant transmissions always affect the aggregating operation, which will affect the convergence. Thus we introduce a regularization term as:

$$\mathcal{L}_\beta = \sum_{s' \in \mathbb{S}} \sum_{s \in \mathbb{S}} \sum_{l \in \mathbb{L}} \sum_{0 \leq l' < l} \ln(1 + \exp^{-\beta_{(s',l') \rightarrow (s,l)}}) / (1 + \exp^{-\beta_{(s',l') \rightarrow (s,l)}}) \quad (8)$$

to help solve this challenge.

- 3 We also want to constrain the minimum and maximum number of fusion modules that connect to it to be 1 and  $k$ , we choose to apply the Lagrangian multiplier method to reformulate such constraints as one regularization term:

$$\begin{aligned} \mathcal{L}_{con} = & \sum_{s \in \mathbb{S}} \sum_{l \in \mathbb{L}} \max(1 - \sum_{s' \in \mathbb{S}} \sum_{l' < l} \frac{1}{1 + \exp^{-\beta_{(s',l') \rightarrow (s,l)}}}, 0) \\ & + \sum_{s \in \mathbb{S}} \sum_{l \in \mathbb{L}} \max(\sum_{s' \in \mathbb{S}} \sum_{l' < l} \frac{1}{1 + \exp^{-\beta_{(s',l') \rightarrow (s,l)}}} - k, 0). \end{aligned} \quad (9)$$

### 3.5 Decoding Network Structure

Once the search procedure terminates, one may derive the suitable operator for each mixture layer and the optimal architecture based on the architecture parameters  $\alpha$  and  $\beta$ . For mixture layer  $\ell_{(s,l)}$ , we select the candidate operation that has maximum operation weight, *i.e.*,  $\arg \max_{o \in \mathcal{O}} \alpha_{(s,l)}^o$ . In terms of the network architecture, we use Breadth-First Search algorithm (see supplemental materials for details) to derive the network architecture in a back to front order.

## 4 Experiments

In this section, we evaluate the performance of DCNAS from various aspects. We first verify the effect of the proxyless searching paradigm by measuring the correlation of the performance between the searching and training environments. Secondly, we quantitatively demonstrate the superiority of DCNAS on several broadly used benchmarks according to corresponding evaluation metrics. Finally, we perform ablation studies to better understand the impact of different design strategies on the semantic image segmentation tasks.

### 4.1 Architecture Search Implementation Details

We first search suitable model structure on Cityscapes [19] dataset and then evaluate this derived model on other benchmarks. In our experiments, for the shape of feature-maps, we set the spatial resolution space  $\mathbb{S}$  to be  $\{1/4, 1/8, 1/16, 1/32\}$ , where each value is a fraction number of spatial resolution and the corresponding widths are set to  $F, 2F, 4F, 8F$ , where we set  $F$  to be 64 for our

best model. Regarding the DCSS, we set the upper-bound of the in-degree of each fusion module  $k$  to be 3 and the hyper-parameter  $L$  to be 14, which are obtained via grid search method [56]. To deliver end-to-end searching and training, we hand-craft a stem module that aims to extract feature-pyramids for DCSS, and we also design a simple prediction head for aggregating all of the feature-maps from DCSS to make the final prediction. For more implementation details, please refer to our supplemental materials.

## 4.2 Correlation of Performance

In this work, we measure NAS methods by quantifying the association of the performance during searching and training configurations. In practice, we take the Spearman's rank correlation coefficient as the evaluation metric and compare our approach with most relevant works [5,6].

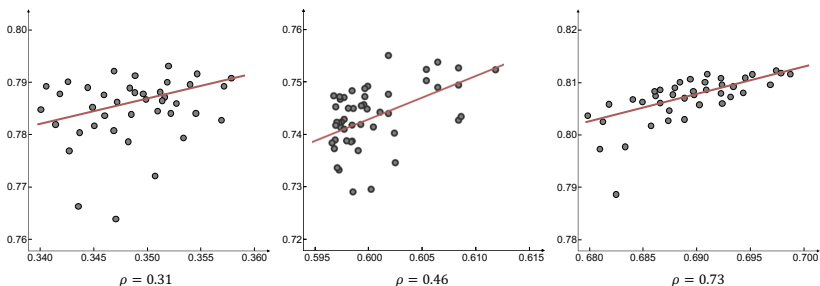


**Fig. 2. Correlation coefficients.** The plots present the quantitative results of Auto-DeepLab [6], DPC [5], and ours (DCNAS) respectively, in which the vertical and horizontal axis represent the validation mIoU in the training and searching phase respectively. We utilize Spearman's rank correlation coefficient ( $\rho$ ) to quantify the correlation of each model's performance between searching and training settings. As we can see, our method achieves a higher correlation coefficient compared with [6,5]. This reveals that the proxyless searching approach comprised in DCNAS is capable of bridging the gap between the searching and the training situations.

To make a fair comparison, we conduct the experiments for 40 times. For each experiment, we run the exploration algorithm on the training dataset of Cityscapes for 80 epochs. After the search procedure terminates, we select the appropriate model by comparing the accuracy of all of temporary models on validation samples and train the derived model for 120 epochs on the training dataset. We report the best validation accuracy of both stages in each experiment for quantitative comparisons. We shall point out that we reproduce the Auto-DeepLab framework based on the officially released code <sup>1</sup>. As to DPC, we refer the announced results from the published paper rather than reproduce the method from scratch due to the intensive computation resource requirements.

<sup>1</sup> <https://github.com/tensorflow/models/tree/master/research/deeplab>

As shown in Figure 2, one can observe that our method obtains a higher validation accuracy in the searching phase compared with [6,5]. This result is reasonable because both [6] and [5] explore the models on a proxy dataset (one with  $321 \times 321$  low-resolution samples, while the other caching the intermediate feature-maps). In contrast, our method does not depend on a proxy dataset, which alleviates the gap between searching and validation data, hence leading to a better performance. Regarding the performance when fine-tuning the derived model, our approach still achieves the best result. This is consistent with our expectation because our search space (DCSS) is more general than [6] and our gradient-based framework is easier to train compared to [5] that rely on Reinforcement Learning. In terms of the quantitative coefficient, our approach outperforms other contemporary methods. It is not astonishing because [6,5] perform the searching with proxy, yet architectures optimized with proxy are not guaranteed to be optimal on the target task. In our case, searching and training environments share the same protocols. Consequently, the paired validation performances shall be approximately linear to a certain extent.

### 4.3 Semantic Segmentation Results

In this section, we evaluate our optimal model structure on Cityscapes [19], PASCAL VOC 2012 [25], ADE20K [31], and PASCAL-Context [32] datasets. We share the same training protocols for all the datasets mentioned above.

**Cityscapes** [19] is a large-scale and challenging dataset, following the conventional evaluation protocol [19], we evaluate our model on 19 semantic labels without considering the void label. Table 1 presents the comparison results of our method and several state-of-the-art methods. Without any pre-training, our base model achieves the performance with 82.8% mIoU<sup>2</sup> on test dataset, which outperforms most state-of-the-art methods [14,15,16,59,60,24,22,23,61,6] and is comparable to [5,21,62]. When training with both train-fine and val-fine sets, our approach attains test performance of 83.1% mIoU, achieving the best result compared with all state-of-the-art methods<sup>3</sup>. Moreover, we can further improve the test mIoU to 83.6<sup>4</sup> when pre-training our model on the Coarse data.

**PASCAL VOC 2012** [25] is another gold-standard benchmark for object segmentation, which contains 20 foreground object classes and one background class. Following conventional [45,14,28,17,6], we exploit the augmented set [71] by pre-training our model on the train + val parts on the augmented set and then fine-tuned on the original Pascal VOC 2012 images. Regarding the track without COCO pretraining, our model advances the new state-of-the-art result to 86.9% mIoU<sup>5</sup>, which largely outperforms the state-of-the-art (absolute 2.5% mIoU improvement). We also plot the per-class comparison in Table 2, one can observe that our model achieves superior performance on many categories (*e.g.*, boat, chair, dog and sofa among 20 classes).

<sup>2</sup> <https://www.cityscapes-dataset.com/anonymous-results/?id=03df3125b090363ed44570b328d73600cc33c6b15f05bc2dce27fad8a8c1f35b>

<sup>3</sup> <https://www.cityscapes-dataset.com/anonymous-results/?id=1918518fd49530f311bf29fee339888348b65d0f18c0dd8495262afdd6fba67a>

<sup>4</sup> <https://www.cityscapes-dataset.com/anonymous-results/?id=2d470c078e787cb6673489f3a4991d87ee5c8b470b1a9bcd970ca34897db1e05>

<sup>5</sup> <http://host.robots.ox.ac.uk:8080/anonymous/PNTTX0.html>

Method	Backbone	Val	Coarse	COCO	ImageNet	mIoU(%)
DepthSeg [57]	Dilated-ResNet-101	✓	✗	✗	✓	78.2
PSPNet [14]	Dilated-ResNet-101	✗	✗	✗	✓	78.4
PAN [29]	Dilated-ResNet-101	✓	✗	✗	✓	78.6
BiSeNet [58]	ResNet-101	✓	✗	✗	✓	78.9
AAF [26]	Dilated-ResNet-101	✗	✗	✗	✓	79.1
DFN [27]	ResNet-101	✓	✗	✗	✓	79.3
CFNet [17]	Dilated-ResNet-101	✓	✗	✓	✓	79.6
PSANet [59]	Dilated-ResNet-101	✓	✗	✗	✓	80.1
PADNet [60]	Dilated-ResNet-101	✓	✗	✗	✓	80.3
Auto-DeepLab [6]	-	✓	✗	✗	✗	80.4
DenseASPP [61]	WDenseNet-161	✓	✗	✗	✓	80.6
SVCNet [23]	ResNet-101	✓	✗	✗	✓	81.0
PSPNet [14]	Dilated-ResNet-101	✓	✓	✗	✓	81.2
DeepLabv3 [15]	ResNet-101	✓	✓	✗	✓	81.3
CCNet [22]	ResNet-101	✓	✗	✗	✓	81.4
DANet [24]	Dilated-ResNet-101	✓	✗	✗	✓	81.5
Mapillary [20]	ResNeXt-101	✓	✓	✗	✓	82.0
DeepLabv3+ [16]	Dilated-ResNet-101	✓	✓	✗	✓	82.1
Auto-DeepLab [6]	-	✓	✓	✗	✗	82.1
DPC [5]	Dilated-Xception-71	✓	✗	✗	✓	82.7
DRN [21]	ResNet-101	✓	✓	✗	✓	82.8
GSCNN [62] †	Wide-ResNet	✓	✗	✗	✓	82.8
Ours (DCNAS) <sup>2</sup>	-	✓	✗	✗	✗	82.8
Ours (DCNAS) <sup>3</sup>	-	✓	✗	✗	✗	83.1
Ours (DCNAS) <sup>4</sup>	-	✓	✓	✗	✗	<b>83.6</b>

**Table 1. Performance on Cityscapes.** The table summarizes the performance on Cityscapes testing dataset. **Val:** Models trained with both train-fine and val-fine parts. **COCO:** Models pre-trained on COCO-stuff dataset. **ImageNet:** The backbones of model trained on ImageNet. **Coarse:** Models that exploit extra datas in Cityscapes with coarse annotation. †: Models pre-trained with the Mapillary Vistas Dataset.

Method	aero	bike	bird	boat	bottle	bus	car	cat	chair	cow	table	dog	horse	mbike	person	plant	sheep	sofa	train	tv	mIoU
FCN [11]	76.8	34.2	68.9	49.4	60.3	75.3	74.7	77.6	21.4	62.5	46.8	71.8	63.9	76.5	73.9	45.2	72.4	37.4	70.9	55.1	62.2
DeepLabv2 [45]	84.4	54.5	81.5	63.6	65.9	85.1	79.1	83.4	30.7	74.1	59.8	79.0	76.1	83.2	80.8	59.7	82.2	50.4	73.1	63.7	71.6
CRF-RNN [53]	87.5	39.0	79.7	64.2	68.3	87.6	80.8	84.4	30.4	78.2	60.4	80.5	77.8	83.1	80.6	59.5	82.8	47.8	75.3	67.1	72.0
DeconNet [64]	89.9	39.3	79.7	63.9	68.2	87.4	81.2	86.1	28.5	77.0	62.0	79.0	80.3	83.6	80.2	58.8	83.4	54.3	80.7	65.0	72.5
GCRF [65]	85.2	43.9	83.3	65.2	68.3	89.0	82.7	85.3	31.1	79.5	63.3	80.5	79.3	85.5	81.0	60.5	85.5	52.0	77.3	65.1	73.2
DFN [66]	87.7	59.4	78.4	64.9	70.3	89.3	83.5	86.1	31.7	79.9	62.6	81.9	80.0	83.5	82.3	60.5	83.2	53.4	77.9	65.0	74.1
Piecewise [42]	90.6	37.6	80.0	67.8	74.4	92.0	85.2	86.2	39.1	81.2	58.9	83.8	85.9	84.1	84.8	62.1	83.2	58.2	80.8	72.3	75.3
AAF [26]	91.2	72.9	90.7	68.2	77.7	95.6	90.7	94.7	40.9	89.5	72.6	91.6	94.1	88.3	88.8	67.3	92.9	62.6	85.2	74.0	82.2
ResNet38 [67]	94.4	72.9	94.9	68.8	78.4	90.6	90.0	92.1	40.1	90.4	71.7	89.9	93.7	91.0	89.1	71.3	90.7	61.3	87.7	78.1	82.5
DANet [24]	-	-	-	-	-	-	-	-	-	-	-	-	-	-	-	-	-	-	-	-	82.6
PSPNet [14]	91.8	71.9	94.7	71.2	75.8	95.2	89.9	95.9	39.3	90.7	71.7	90.5	94.5	88.8	89.6	72.8	89.6	64.0	85.1	76.3	82.6
DFN [27]	-	-	-	-	-	-	-	-	-	-	-	-	-	-	-	-	-	-	-	-	82.7
EncNet [28]	94.1	69.2	96.3	76.7	86.2	96.3	90.7	94.2	38.8	90.7	73.3	90.0	92.5	88.8	87.9	68.7	92.6	59.0	86.4	71.4	82.9
PAN [29]	95.7	75.2	94.0	73.8	79.6	96.5	93.7	94.1	40.5	93.3	72.4	89.1	94.1	91.6	89.5	73.6	93.2	62.8	87.3	78.6	84.0
CFNet [17]	95.7	71.9	95.0	76.3	82.8	94.8	90.0	95.9	37.1	92.6	73.0	93.4	94.6	89.6	88.4	74.9	95.2	63.2	89.7	78.2	84.2
APCNet [33]	95.8	75.8	84.5	76.0	80.6	95.9	90.0	96.0	42.0	93.7	75.4	91.6	95.0	90.5	89.3	75.8	92.8	61.9	83.9	79.6	84.2
DMNet [30]	96.1	77.3	94.1	72.8	78.1	97.1	92.7	96.4	39.8	91.4	75.5	92.7	95.8	91.0	90.3	76.6	94.1	62.1	85.5	77.6	84.4
Ours (DCNAS) <sup>5</sup>	96.5	75.2	96.1	80.7	85.2	97.0	93.8	96.6	49.5	94.0	77.6	95.1	95.7	93.9	89.7	76.1	94.7	70.9	89.7	79.4	86.9

**Table 2. Performance on PASCAL VOC 2012.** The table presents per-class semantic segmentation results on the PASCAL VOC 2012 test dataset (track without coco pre-training). Our method advances the new state-of-the-art with mIoU 86.9%

**Pascal Context [32]** and **ADE20K [31]** are standard benchmarks toward scene parsing tasks. Being consistent with [17,22,72,6], we employ not only the classical mIoU but also the pixel accuracy as the evaluation metrics for ADE20K. As to Pascal Context, we report the mIoUs both with (60-cls) and without (59-cls) considering the background. As shown in Table 3, we present the performances of our model on the validation parts of Pascal Context and ADE20K

Methods	ADE20K		Pascal Context	
	mIoU	Pix-Acc	mIoU 59-cls	mIoU 60-cls
DeepLabv2 [45]	-	-	-	45.7
GCPNet [68]	38.37	77.76	-	46.5
RefineNet [47]	40.70	-	-	47.3
MSCI [69]	-	-	-	50.3
PSANet [59]	43.77	81.51	-	-
PSPNet [14]	44.94	81.69	47.8	-
SAC [34]	44.30	-	-	-
CCL [70]	-	-	-	51.6
EncNet [28]	44.65	81.69	52.6	51.7
DSSPN [35]	43.68	-	-	-
CFNet [17]	44.89	-	54.0	-
CCNet [22]	45.22	-	-	-
DeepLabv3+ [16]	45.65	82.52	-	-
Auto-DeepLab [6]	43.98	81.72	-	-
APCNet [33]	45.38	-	55.6	54.7
DANet [24]	-	-	-	52.6
SVCNet [23]	-	-	53.2	-
DRN [21]	-	-	49.0	-
Ours (DCNAS)	<b>47.12</b>	<b>84.31</b>	<b>57.1</b>	<b>55.6</b>

**Table 3. Performance on ADE20K and Pascal Context.** The table presents the semantic segmentation performance on the validation part of ADE20K and Pascal Context according to various evaluation metrics.

according to corresponding evaluation metrics. Our DCNAS outperforms other state-of-the-art methods on both Pascal Context and ADE20K datasets.

It is consistent with our expectation that our approach retained leading performance on the above mentioned extensively used benchmarks with various evaluation metrics. Specifically: (1) the proxyless searching paradigm can bridge the gap between searching and training environments, which is conducive to the discovery of promising model structures; (2) our DCNAS includes an abundance of possible model structures, accompanied with the proxyless searching method, so that one may easily obtain an outstanding model; (3) the multi-scale semantic features aggregation has been proved to be instrumental for visual recognition [11,45,14,16,62], and our DCNAS inherently and repeatedly applying top-down and bottom-up multi-scale features fusion, hence results in leading performance.

#### 4.4 Ablation Study

To better understand the impact of different design choices, we evaluate our framework in various settings. Two main design choices exist in this work, the impact of hyper-parameters  $L$  and  $k$ , and the effect of the novel regularization terms. We still take the mIoU as the evaluation metric for searching (S-mIoU) and training (T-mIoU) periods on the validation dataset of the Cityscapes.

In Table 4, one may observe that for a fixed  $k$ , the performance improves as the hyper-parameter  $L$  increases, which is reasonable since  $L$  is closely correlated to the capacity of the model. Besides, for a fixed  $L$ , as  $k$  increases, the performance grows first and then decreases, because that for larger  $k$ , the model may get stuck in a local optimal state thereby leading to unsatisfactory performance.

$L$	$k$	S-mIoU	T-mIoU
8	4	60.3	72.7
12	4	64.7	77.8
14	4	69.6	81.0
16	4	<b>69.9</b>	<b>81.1</b>
14	1	59.4	76.2
14	2	66.8	79.5
14	3	69.7	<b>81.1</b>
14	5	69.3	80.9

**Table 4. Ablation Study.** We present the performance of our DCNAS on Cityscapes validation dataset with varying configurations of  $L$  and  $k$ .

$\mathcal{L}_{con}$	$\mathcal{L}_\beta$	$\mathcal{L}_\alpha$	S-mIoU	T-mIoU
$\times$	$\times$	$\times$	48.1	76.5
$\times$	$\times$	$\checkmark$	51.3	77.1
$\times$	$\checkmark$	$\times$	63.9	79.4
$\times$	$\checkmark$	$\checkmark$	65.3	79.9
$\checkmark$	$\times$	$\times$	55.2	78.3
$\checkmark$	$\times$	$\checkmark$	58.7	78.4
$\checkmark$	$\checkmark$	$\times$	69.6	80.9
$\checkmark$	$\checkmark$	$\checkmark$	<b>69.9</b>	<b>81.2</b>

**Table 5. Ablation Studies.** We investigate the impact of different regularization terms by comparing the performance on Cityscapes validation set, in which  $L$  and  $k$  are set to be 14 and 3.

Considering the phenomenons mentioned above, we set the hyper-parameters  $L$  and  $k$  to be 14 and 3 respectively, for our benchmark model.

Regarding the regularization terms, we observe that the  $\mathcal{L}_\beta$  is crucial to performance improvement, and adding the regularization term  $\mathcal{L}_{con}$  can yield marginal performance improvement. We think there are two reasons: (1) the regularization term  $\mathcal{L}_\beta$  forces the relaxed continuous representations of path connection to be 0 or 1, which stabilizes the network architecture; (2) constraint  $\mathcal{L}_{con}$  helps prune insignificant path-level connections and derive a sparse model structure, which further stabilizes the network architecture. Moreover, as presented in Table 5, adding the regularization term  $\mathcal{L}_\alpha$  can further improve the performance, since  $\mathcal{L}_\alpha$  leads to a discrete distribution of operator space in each mixture-layer, which yields more stable and reliable training.

## 5 Conclusion

In this work, we propose a novel NAS framework, namely DCNAS, to directly and proxylessly search the optimal multi-scale network architectures for dense image prediction tasks. We introduce a densely connected search space (DCSS), which contains most of the widespread human-designed network structures. With DCSS, we may be the first one to attempt to fully automatically search the optimal multi-scale representations of high-resolution imagery and to fuse those multi-scale features. Meanwhile, to enable the efficient searching process, we propose a fusion module to deal with the high GPU memory consumption and expensive computation overhead issues. Consequently, we implement the first proxyless NAS framework for dense image prediction tasks, which demand multi-scale features representation to achieve the-state-of-art performance. Experiment results demonstrate that the architectures obtained from our DCNAS can surpass not only the human-invented architectures but also the automatically designed architectures from previous NAS methods. For future work, we hope the ideas delivered from our DCNAS, ample search space and fusion module, can be applied to other dense image prediction tasks.

## References

1. Zoph, B., Le, Q.V.: Neural architecture search with reinforcement learning. arXiv preprint arXiv:1611.01578 (2016)
2. Zoph, B., Vasudevan, V., Shlens, J., Le, Q.V.: Learning transferable architectures for scalable image recognition. In: Proceedings of the IEEE conference on computer vision and pattern recognition. (2018) 8697–8710
3. Liu, H., Simonyan, K., Vinyals, O., Fernando, C., Kavukcuoglu, K.: Hierarchical representations for efficient architecture search. arXiv preprint arXiv:1711.00436 (2017)
4. Liu, H., Simonyan, K., Yang, Y.: Darts: Differentiable architecture search. arXiv preprint arXiv:1806.09055 (2018)
5. Chen, L.C., Collins, M., Zhu, Y., Papandreou, G., Zoph, B., Schroff, F., Adam, H., Shlens, J.: Searching for efficient multi-scale architectures for dense image prediction. In: Advances in neural information processing systems. (2018) 8699–8710
6. Liu, C., Chen, L.C., Schroff, F., Adam, H., Hua, W., Yuille, A.L., Fei-Fei, L.: Auto-deeplab: Hierarchical neural architecture search for semantic image segmentation. In: Proceedings of the IEEE Conference on Computer Vision and Pattern Recognition. (2019) 82–92
7. Wu, H., Zhang, J., Huang, K.: Sparsemask: Differentiable connectivity learning for dense image prediction. In: Proceedings of the IEEE International Conference on Computer Vision. (2019) 6768–6777
8. Nekrasov, V., Chen, H., Shen, C., Reid, I.: Fast neural architecture search of compact semantic segmentation models via auxiliary cells. In: Proceedings of the IEEE Conference on Computer Vision and Pattern Recognition. (2019) 9126–9135
9. Shaw, A., Hunter, D., Landola, F., Sidhu, S.: Squeezenas: Fast neural architecture search for faster semantic segmentation. In: Proceedings of the IEEE International Conference on Computer Vision Workshops. (2019) 0–0
10. Li, X., Zhou, Y., Pan, Z., Feng, J.: Partial order pruning: for best speed/accuracy trade-off in neural architecture search. In: Proceedings of the IEEE Conference on Computer Vision and Pattern Recognition. (2019) 9145–9153
11. Long, J., Shelhamer, E., Darrell, T.: Fully convolutional networks for semantic segmentation. In: Proceedings of the IEEE conference on computer vision and pattern recognition. (2015) 3431–3440
12. Newell, A., Yang, K., Deng, J.: Stacked hourglass networks for human pose estimation. In: European conference on computer vision, Springer (2016) 483–499
13. Liu, W., Rabinovich, A., Berg, A.C.: Parsenet: Looking wider to see better. arXiv preprint arXiv:1506.04579 (2015)
14. Zhao, H., Shi, J., Qi, X., Wang, X., Jia, J.: Pyramid scene parsing network. In: Proceedings of the IEEE conference on computer vision and pattern recognition. (2017) 2881–2890
15. Chen, L.C., Papandreou, G., Schroff, F., Adam, H.: Rethinking atrous convolution for semantic image segmentation. arXiv preprint arXiv:1706.05587 (2017)
16. Chen, L.C., Zhu, Y., Papandreou, G., Schroff, F., Adam, H.: Encoder-decoder with atrous separable convolution for semantic image segmentation. In: Proceedings of the European conference on computer vision (ECCV). (2018) 801–818
17. Zhang, H., Zhang, H., Wang, C., Xie, J.: Co-occurrent features in semantic segmentation. In: Proceedings of the IEEE Conference on Computer Vision and Pattern Recognition. (2019) 548–557

18. Cai, H., Zhu, L., Han, S.: Proxylessnas: Direct neural architecture search on target task and hardware. arXiv preprint arXiv:1812.00332 (2018)
19. Cordts, M., Omran, M., Ramos, S., Rehfeld, T., Enzweiler, M., Benenson, R., Franke, U., Roth, S., Schiele, B.: The cityscapes dataset for semantic urban scene understanding. In: Proceedings of the IEEE conference on computer vision and pattern recognition. (2016) 3213–3223
20. Rota Bulò, S., Porzi, L., Kotschieder, P.: In-place activated batchnorm for memory-optimized training of dnns. In: Proceedings of the IEEE Conference on Computer Vision and Pattern Recognition. (2018) 5639–5647
21. Zhuang, Y., Yang, F., Tao, L., Ma, C., Zhang, Z., Li, Y., Jia, H., Xie, X., Gao, W.: Dense relation network: Learning consistent and context-aware representation for semantic image segmentation. In: 2018 25th IEEE international conference on image processing (ICIP), IEEE (2018) 3698–3702
22. Huang, Z., Wang, X., Huang, L., Huang, C., Wei, Y., Liu, W.: Ccnet: Criss-cross attention for semantic segmentation. In: Proceedings of the IEEE International Conference on Computer Vision. (2019) 603–612
23. Ding, H., Jiang, X., Shuai, B., Liu, A.Q., Wang, G.: Semantic correlation promoted shape-variant context for segmentation. In: Proceedings of the IEEE Conference on Computer Vision and Pattern Recognition. (2019) 8885–8894
24. Fu, J., Liu, J., Tian, H., Li, Y., Bao, Y., Fang, Z., Lu, H.: Dual attention network for scene segmentation. In: Proceedings of the IEEE Conference on Computer Vision and Pattern Recognition. (2019) 3146–3154
25. Everingham, M., Van Gool, L., Williams, C.K., Winn, J., Zisserman, A.: The pascal visual object classes (voc) challenge. International journal of computer vision **88**(2) (2010) 303–338
26. Ke, T.W., Hwang, J.J., Liu, Z., Yu, S.X.: Adaptive affinity fields for semantic segmentation. In: Proceedings of the European Conference on Computer Vision (ECCV). (2018) 587–602
27. Yu, C., Wang, J., Peng, C., Gao, C., Yu, G., Sang, N.: Learning a discriminative feature network for semantic segmentation. In: Proceedings of the IEEE conference on computer vision and pattern recognition. (2018) 1857–1866
28. Zhang, H., Dana, K., Shi, J., Zhang, Z., Wang, X., Tyagi, A., Agrawal, A.: Context encoding for semantic segmentation. In: Proceedings of the IEEE conference on Computer Vision and Pattern Recognition. (2018) 7151–7160
29. Li, H., Xiong, P., An, J., Wang, L.: Pyramid attention network for semantic segmentation. arXiv preprint arXiv:1805.10180 (2018)
30. He, J., Deng, Z., Qiao, Y.: Dynamic multi-scale filters for semantic segmentation. In: Proceedings of the IEEE International Conference on Computer Vision. (2019) 3562–3572
31. Zhou, B., Zhao, H., Puig, X., Fidler, S., Barriuso, A., Torralba, A.: Scene parsing through ade20k dataset. In: Proceedings of the IEEE conference on computer vision and pattern recognition. (2017) 633–641
32. Mottaghi, R., Chen, X., Liu, X., Cho, N.G., Lee, S.W., Fidler, S., Urtasun, R., Yuille, A.: The role of context for object detection and semantic segmentation in the wild. In: Proceedings of the IEEE Conference on Computer Vision and Pattern Recognition. (2014) 891–898
33. He, J., Deng, Z., Zhou, L., Wang, Y., Qiao, Y.: Adaptive pyramid context network for semantic segmentation. In: Proceedings of the IEEE Conference on Computer Vision and Pattern Recognition. (2019) 7519–7528



34. Zhang, R., Tang, S., Zhang, Y., Li, J., Yan, S.: Scale-adaptive convolutions for scene parsing. In: Proceedings of the IEEE International Conference on Computer Vision. (2017) 2031–2039
35. Liang, X., Zhou, H., Xing, E.: Dynamic-structured semantic propagation network. In: Proceedings of the IEEE Conference on Computer Vision and Pattern Recognition. (2018) 752–761
36. Real, E., Moore, S., Selle, A., Saxena, S., Suematsu, Y.L., Tan, J., Le, Q.V., Kurakin, A.: Large-scale evolution of image classifiers. In: Proceedings of the 34th International Conference on Machine Learning-Volume 70, JMLR. org (2017) 2902–2911
37. Pham, H., Guan, M.Y., Zoph, B., Le, Q.V., Dean, J.: Efficient neural architecture search via parameter sharing. arXiv preprint arXiv:1802.03268 (2018)
38. Tan, M., Chen, B., Pang, R., Vasudevan, V., Sandler, M., Howard, A., Le, Q.V.: Mnasnet: Platform-aware neural architecture search for mobile. In: Proceedings of the IEEE Conference on Computer Vision and Pattern Recognition. (2019) 2820–2828
39. Wu, B., Dai, X., Zhang, P., Wang, Y., Sun, F., Wu, Y., Tian, Y., Vajda, P., Jia, Y., Keutzer, K.: Fbnet: Hardware-aware efficient convnet design via differentiable neural architecture search. In: Proceedings of the IEEE Conference on Computer Vision and Pattern Recognition. (2019) 10734–10742
40. Chen, X., Xie, L., Wu, J., Tian, Q.: Progressive differentiable architecture search: Bridging the depth gap between search and evaluation. In: Proceedings of the IEEE International Conference on Computer Vision. (2019) 1294–1303
41. Fang, J., Sun, Y., Zhang, Q., Li, Y., Liu, W., Wang, X.: Densely connected search space for more flexible neural architecture search. arXiv preprint arXiv:1906.09607 (2019)
42. Lin, G., Shen, C., Van Den Hengel, A., Reid, I.: Efficient piecewise training of deep structured models for semantic segmentation. In: Proceedings of the IEEE conference on computer vision and pattern recognition. (2016) 3194–3203
43. Chen, L.C., Yang, Y., Wang, J., Xu, W., Yuille, A.L.: Attention to scale: Scale-aware semantic image segmentation. In: Proceedings of the IEEE conference on computer vision and pattern recognition. (2016) 3640–3649
44. Eigen, D., Fergus, R.: Predicting depth, surface normals and semantic labels with a common multi-scale convolutional architecture. In: Proceedings of the IEEE international conference on computer vision. (2015) 2650–2658
45. Chen, L.C., Papandreou, G., Kokkinos, I., Murphy, K., Yuille, A.L.: Deeplab: Semantic image segmentation with deep convolutional nets, atrous convolution, and fully connected crfs. *IEEE transactions on pattern analysis and machine intelligence* **40**(4) (2017) 834–848
46. Ronneberger, O., Fischer, P., Brox, T.: U-net: Convolutional networks for biomedical image segmentation. In: International Conference on Medical image computing and computer-assisted intervention, Springer (2015) 234–241
47. Lin, G., Milan, A., Shen, C., Reid, I.: Refinenet: Multi-path refinement networks for high-resolution semantic segmentation. In: Proceedings of the IEEE conference on computer vision and pattern recognition. (2017) 1925–1934
48. Pohlen, T., Hermans, A., Mathias, M., Leibe, B.: Full-resolution residual networks for semantic segmentation in street scenes. In: Proceedings of the IEEE Conference on Computer Vision and Pattern Recognition. (2017) 4151–4160
49. Fu, J., Liu, J., Wang, Y., Zhou, J., Wang, C., Lu, H.: Stacked deconvolutional network for semantic segmentation. *IEEE Transactions on Image Processing* (2019)

50. Chen, W., Gong, X., Liu, X., Zhang, Q., Li, Y., Wang, Z.: Fasterseg: Searching for faster real-time semantic segmentation. arXiv preprint arXiv:1912.10917 (2019)
51. Zhang, Y., Qiu, Z., Liu, J., Yao, T., Liu, D., Mei, T.: Customizable architecture search for semantic segmentation. In: Proceedings of the IEEE Conference on Computer Vision and Pattern Recognition. (2019) 11641–11650
52. Howard, A., Sandler, M., Chu, G., Chen, L.C., Chen, B., Tan, M., Wang, W., Zhu, Y., Pang, R., Vasudevan, V., et al.: Searching for mobilenetv3. arXiv preprint arXiv:1905.02244 (2019)
53. Baker, B., Gupta, O., Naik, N., Raskar, R.: Designing neural network architectures using reinforcement learning. arXiv preprint arXiv:1611.02167 (2016)
54. Suganuma, M., Shirakawa, S., Nagao, T.: A genetic programming approach to designing convolutional neural network architectures. In: Proceedings of the Genetic and Evolutionary Computation Conference. (2017) 497–504
55. Xie, S., Zheng, H., Liu, C., Lin, L.: Snas: stochastic neural architecture search. arXiv preprint arXiv:1812.09926 (2018)
56. Bergstra, J., Bengio, Y.: Random search for hyper-parameter optimization. *Journal of machine learning research* **13**(Feb) (2012) 281–305
57. Kong, S., Fowlkes, C.C.: Recurrent scene parsing with perspective understanding in the loop. In: Proceedings of the IEEE Conference on Computer Vision and Pattern Recognition. (2018) 956–965
58. Yu, C., Wang, J., Peng, C., Gao, C., Yu, G., Sang, N.: Bisenet: Bilateral segmentation network for real-time semantic segmentation. In: Proceedings of the European conference on computer vision (ECCV). (2018) 325–341
59. Zhao, H., Zhang, Y., Liu, S., Shi, J., Change Loy, C., Lin, D., Jia, J.: Psanet: Point-wise spatial attention network for scene parsing. In: Proceedings of the European Conference on Computer Vision (ECCV). (2018) 267–283
60. Xu, D., Ouyang, W., Wang, X., Sebe, N.: Pad-net: Multi-tasks guided prediction-and-distillation network for simultaneous depth estimation and scene parsing. In: Proceedings of the IEEE Conference on Computer Vision and Pattern Recognition. (2018) 675–684
61. Yang, M., Yu, K., Zhang, C., Li, Z., Yang, K.: Denseaspp for semantic segmentation in street scenes. In: Proceedings of the IEEE Conference on Computer Vision and Pattern Recognition. (2018) 3684–3692
62. Takikawa, T., Acuna, D., Jampani, V., Fidler, S.: Gated-scnn: Gated shape cnns for semantic segmentation. In: Proceedings of the IEEE International Conference on Computer Vision. (2019) 5229–5238
63. Zheng, S., Jayasumana, S., Romera-Paredes, B., Vineet, V., Su, Z., Du, D., Huang, C., Torr, P.H.: Conditional random fields as recurrent neural networks. In: Proceedings of the IEEE international conference on computer vision. (2015) 1529–1537
64. Noh, H., Hong, S., Han, B.: Learning deconvolution network for semantic segmentation. In: Proceedings of the IEEE international conference on computer vision. (2015) 1520–1528
65. Vemulapalli, R., Tuzel, O., Liu, M.Y., Chellapa, R.: Gaussian conditional random field network for semantic segmentation. In: Proceedings of the IEEE conference on computer vision and pattern recognition. (2016) 3224–3233
66. Liu, Z., Li, X., Luo, P., Loy, C.C., Tang, X.: Semantic image segmentation via deep parsing network. In: Proceedings of the IEEE international conference on computer vision. (2015) 1377–1385
67. Wu, Z., Shen, C., Van Den Hengel, A.: Wider or deeper: Revisiting the resnet model for visual recognition. *Pattern Recognition* **90** (2019) 119–133

68. Hung, W.C., Tsai, Y.H., Shen, X., Lin, Z., Sunkavalli, K., Lu, X., Yang, M.H.: Scene parsing with global context embedding. In: Proceedings of the IEEE International Conference on Computer Vision. (2017) 2631–2639
69. Lin, D., Ji, Y., Lischinski, D., Cohen-Or, D., Huang, H.: Multi-scale context intertwining for semantic segmentation. In: Proceedings of the European Conference on Computer Vision (ECCV). (2018) 603–619
70. Ding, H., Jiang, X., Shuai, B., Qun Liu, A., Wang, G.: Context contrasted feature and gated multi-scale aggregation for scene segmentation. In: Proceedings of the IEEE Conference on Computer Vision and Pattern Recognition. (2018) 2393–2402
71. Hariharan, B., Arbeláez, P., Bourdev, L., Maji, S., Malik, J.: Semantic contours from inverse detectors. In: 2011 International Conference on Computer Vision, IEEE (2011) 991–998
72. Zhu, Z., Xu, M., Bai, S., Huang, T., Bai, X.: Asymmetric non-local neural networks for semantic segmentation. In: Proceedings of the IEEE International Conference on Computer Vision. (2019) 593–602